

Logarithmic Accuracy of Angular-Ordered Parton Showers

**Gavin Bewick^a Silvia Ferrario Ravasio^a Peter Richardson^{a,b}
Michael H. Seymour^c**

^a*Institute for Particle Physics Phenomenology, Durham University*

^b*Theoretical Physics Department, CERN, Switzerland*

^c*Lancaster-Manchester-Sheffield Consortium for Fundamental Physics, School of Physics and Astronomy, University of Manchester, M13 9PL, U.K.*

E-mail: gavin.bewick@durham.ac.uk,
silvia.ferrario-ravasio@durham.ac.uk,
peter.richardson@durham.ac.uk, Michael.Seymour@manchester.ac.uk

ABSTRACT: We study the logarithmic accuracy of angular-ordered parton showers by considering the singular limits of multiple emission matrix elements. This allows us to consider different choices for the evolution variable and propose a new choice which has both the correct logarithmic behaviour and improved performance away from the singular regions. In particular the description of e^+e^- event shapes in the non-logarithmic region is significantly improved.

Contents

1	Introduction	1
2	Kinematics	3
2.1	Single Emission	4
2.2	Second emission	4
3	Interpretation of the Evolution Variable	5
3.1	p_T preserving scheme	6
3.2	q^2 preserving scheme	6
3.3	Dot-product preserving scheme	6
3.3.1	Phase-space corrections	8
4	Logarithmic accuracy	10
4.1	p_T preserving scheme	11
4.2	q^2 preserving scheme	13
4.3	Dot-product preserving scheme	14
4.4	Global recoil	15
5	Tuning	17
6	Results	18
6.1	LEP results	19
6.2	LHC results	21
7	Conclusions	22
A	$g \rightarrow q\bar{q}$ branching in the dot-product preserving scheme	23

1 Introduction

Monte Carlo event generators [1–4], which provide a complete description of the complicated hadronic final state observed in high-energy particle collisions, are essential tools as their results can be directly compared with experimental measurements. These simulations combine a calculation of the hard scattering process, usually at next-to-leading order accuracy, with parton shower (PS) evolution from the scale of the hard process to a low energy scale where non-perturbative hadronization models describe the formation of hadrons from the quarks and gluons of the perturbative

calculation. Together with a non-perturbative model of multiple parton scattering and decay of the primary hadrons, these generators simulate the final hadronic state.¹

Most of the progress made in this field over the last decade came from matching the parton shower approximation of QCD radiation with fixed-order matrix elements. This increased the accuracy of the cross-section calculation and improved the description of hard radiation, which is not adequately described by the soft and collinear approximations used in parton shower algorithms. In the last few years however there has been a revival of work [6–9] to improve the accuracy of the parton shower algorithm in antenna [10–12] and dipole [13–15] showers, as well as work on amplitude-based evolution to treat subleading colour effects [16, 17].

A recent work [18] showed that two popular dipole shower algorithms, that of PYTHIA 8 [19] and Dire [20], have issues even at leading-logarithmic accuracy due to the way the singular emissions are split between different dipole contributions and how recoils are handled. The authors considered an initial $q\bar{q}$ dipole and the emission of two gluons g_1 and g_2 that are both soft and collinear to either of the hard partons and widely separated in rapidity from each other. Given these requirements, the two emissions must be independent and the double-emission probability is

$$dP_{\text{soft}}^{(2)} = \frac{1}{2!} \prod_{i=1}^2 \left[C_F \frac{\alpha_s(p_{Ti})}{2\pi} \frac{d\phi_i}{2\pi} \frac{dp_{Ti}^2}{p_{Ti}^2} dy_i \right], \quad (1.1)$$

where y_i is the rapidity of the gluon i and p_{Ti} is its transverse momentum, all computed in the original $q\bar{q}$ dipole frame, where the z axis is aligned with the q direction. The second gluon, g_2 , can be emitted either from the $\bar{q} - g_1$ or from the $q - g_1$ dipole. However, although g_2 may be further from g_1 than g_1 is from one of the two hard partons, when the event is looked at in the emitting-dipole frame, it may happen that g_2 becomes closer in angle to g_1 , which will thus play the role of the emitter. This leads to the assignment of the incorrect colour factor $C_A/2$ instead of C_F . This mistake has no effect at leading colour, since $C_F \rightarrow C_A/2$ in the large number of colours limit, but corresponds to an error in the subleading colour contribution. Furthermore, if g_1 is identified as the emitting particle in the emitting dipole, it has to balance the transverse momentum of g_2 and

$$\mathbf{p}_{T1} \rightarrow \mathbf{p}_{T1} - \mathbf{p}_{T2}, \quad (1.2)$$

where the bold symbol indicates it is a two-momentum. This implies that p_{T1} can receive a substantial modification if the transverse momentum of the second gluon is only marginally smaller than that of the first emission, thus violating Eqn. (1.1).

In this paper we will use a similar approach to that of Ref. [18] in order to analyse the behaviour of the improved angular-ordered shower of Ref. [21]. Although it is clear that the subleading colour issue will not affect an angular-ordered

¹For a complete review of the approximations and models used see ref. [5].

parton shower, the effect of the recoil must be carefully taken into account. The angular-order parton shower, which uses on a “global” recoil and $1 \rightarrow 2$ splittings is significantly different from the dipole showers, which implement “local” recoil, and were considered in Ref. [18]. This means that while some of the issues considered in Ref. [18] are irrelevant for parton showers using $1 \rightarrow 2$ kinematics and global recoil, some of the underlying physics issues addressed can occur in the angular-ordered parton shower, although they manifest themselves in different ways.

In the next section we present the definitions of the parton momenta and kinematics used in the angular-ordered parton shower. These are then used to construct three different interpretations of the evolution variable and consider the logarithmic accuracy of each. To ensure a like-for-like comparison between new and old evolution variables we tune the Herwig 7 angular-ordered parton shower for all of them. Finally we present our conclusions.

2 Kinematics

We will define all momenta in terms of the Sudakov basis such that the 4-momentum of particle l is

$$q_l = \alpha_l p + \beta_l n + k_{\perp l}, \quad (2.1)$$

where the reference vectors p and n obey

$$p^2 = m_0^2, \quad p \cdot n \neq 0, \quad n^2 = 0, \quad p \cdot k_{\perp l} = n \cdot k_{\perp l} = 0, \quad (2.2)$$

and the transverse momentum 4-vector $k_{\perp l}$ is spacelike.

For many results we will not need a specific representation of the reference vectors. If we need a representation we will use the choice made in Ref. [21] for final-state radiation with a final-state colour partner, *i.e.*

$$p = \frac{Q}{2} [1 + b - c, 0, 0, \lambda]; \quad (2.3a)$$

$$n = \frac{Q}{2} [\lambda, 0, 0, -\lambda]; \quad (2.3b)$$

where Q is the invariant mass of the radiating particle and its colour partner, $b = m_0^2/Q^2$, $c = m_s^2/Q^2$, λ is the Källén function

$$\lambda(1, b, c) = \sqrt{1 + b^2 + c^2 - 2b - 2c - 2bc}, \quad (2.4)$$

and m_0 , m_s are the masses of the radiating particle and its colour partner, respectively.

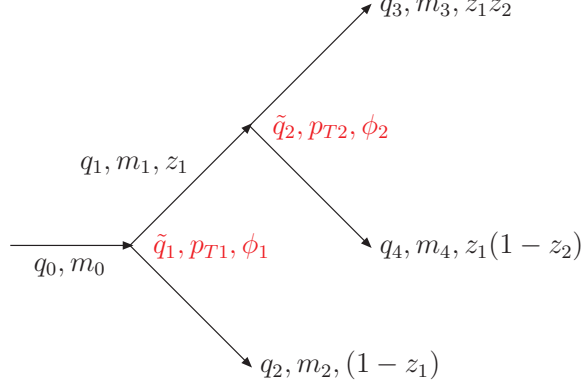


Figure 1. The kinematics of two branchings in the angular-ordered parton shower. The off-shell momentum (q_i), on-shell masses (m_i) and light-cone momentum fractions of the partons are shown together with the evolution variable (\tilde{q}_i), transverse momentum (p_{T_i}) and azimuthal angles (ϕ_i) of the two branchings.

2.1 Single Emission

For the branching $0 \rightarrow 12$, with no further emission we have:

$$q_0 = p + \beta_0 n; \quad (2.5a)$$

$$q_1 = zp + \beta_1 n + q_\perp; \quad (2.5b)$$

$$q_2 = (1 - z)p + \beta_2 n - q_\perp; \quad (2.5c)$$

where z is the light-cone momentum fraction, q_\perp the transverse momentum 4-vector, $m_{0,1,2}$ are the on-shell masses of the particles, $\beta_{1,2}$ are determined by the on-shell condition $q_{1,2}^2 = m_{1,2}^2$ and β_0 by momentum conservation. The virtuality of the parton initiating the branching is therefore

$$q_0^2 = \frac{p_T^2}{z(1-z)} + \frac{m_1^2}{z} + \frac{m_2^2}{(1-z)}, \quad (2.6)$$

where $q_\perp^2 = -p_T^2$.

2.2 Second emission

If we consider two emissions, the first with z_1, \tilde{q}_1, ϕ_1 and the second from the first outgoing parton of the first branching with z_2, \tilde{q}_2, ϕ_2 , as shown in Fig. 1.

We define the off-shell momenta of the four partons after the branchings as:

$$q_0 = p + \beta_0 n; \quad (2.7a)$$

$$q_1 = z_1 p + \beta_1 n + q_{\perp 1}; \quad (2.7b)$$

$$q_2 = (1 - z_1)p + \beta_2 n - q_{\perp 1}; \quad (2.7c)$$

$$q_3 = z_1 z_2 p + \beta_3 n + z_2 q_{\perp 1} + q_{\perp 2}; \quad (2.7d)$$

$$q_4 = z_1(1 - z_2)p + \beta_4 n + (1 - z_2)q_{\perp 1} - q_{\perp 2}; \quad (2.7e)$$

where $p^2 = m_0^2$, the β_i coefficients are fixed by the on-shell condition and momentum conservation and the space-like transverse momentum

$$q_{\perp i} = [0; \mathbf{p}_{T_i}, 0] = [0; p_{T_i} \cos \phi_i, p_{T_i} \sin \phi_i, 0], \quad (2.8)$$

such that $q_{\perp i}^2 = -\mathbf{p}_{T_i}^2 = -p_{T_i}^2$. The virtualities of the branching partons are:

$$q_0^2 = \frac{p_{T1}^2}{z_1(1-z_1)} + \frac{q_1^2}{z_1} + \frac{m_2^2}{1-z_1}; \quad (2.9a)$$

$$q_1^2 = \frac{p_{T2}^2}{z_2(1-z_2)} + \frac{m_3^2}{z_2} + \frac{m_4^2}{1-z_2}. \quad (2.9b)$$

In all the cases we will consider parton 4 will be a gluon, $m_4 = 0$, so that partons 1 and 3 must have the same mass, *i.e.* $m_1 = m_3$. It will also prove useful to define a unit vector in the direction of the transverse momentum, *i.e.*

$$\hat{\mathbf{n}}_i = [\cos \phi_i, \sin \phi_i]. \quad (2.10)$$

3 Interpretation of the Evolution Variable

In Ref. [21] the extension of the original angular-ordered parton shower [22] to include mass effects and longitudinal boost invariance along the jet axis was presented. In this algorithm the evolution variable is

$$\tilde{q}^2 = \frac{q_0^2 - m_0^2}{z(1-z)}, \quad (3.1)$$

in order to include masses effects, in particular the correct mass in the propagator, retain angular-ordering and have a simple single emission probability

$$d\mathcal{P} = \frac{d\tilde{q}^2}{\tilde{q}^2} \frac{\alpha_S}{2\pi} \frac{d\phi}{2\pi} dz P_{i \rightarrow jk}(z, \tilde{q}), \quad (3.2)$$

where $P_{i \rightarrow jk}(z, \tilde{q})$ is the quasi-collinear splitting function [23], z is the light-cone momentum fraction and ϕ is the azimuthal angle of the transverse momentum generated in the splitting. The strong coupling α_S is evaluated at the transverse momentum of the splitting [24, 25].

For a single emission (or the last emission in an extended shower) where the children are on their mass-shell, the kinematics are unambiguously defined by Eqn. 3.1. However, when the children of a branching go on to branch further so that they are off-shell, there is room for different interpretations of \tilde{q}^2 , *i.e.* different determinations of the kinematics from it. The procedure used by **Herwig** is to first generate a value of \tilde{q}^2 (and z) for a branching and calculate a kinematic variable from them (the choice of which kinematic variable will be discussed below). Then the upper limit of \tilde{q}^2 is

calculated for each of the children and they are fully evolved. Finally, the generation of this branching is completed by constructing its kinematics from its (now off-shell) children's momenta, using the kinematic variable that had been constructed from \tilde{q}^2 . Thus any other kinematic variables are shifted slightly, to accommodate the change from on-shell to off-shell kinematics.

We will investigate three different choices for the kinematic variable that is preserved.

3.1 p_T preserving scheme

The original choice of Ref. [21] was to use Eqn. 3.1 together with the expression of the virtuality in Eqn. 2.6, to define the transverse momentum of the branching $0 \rightarrow 12$,

$$p_T^2 = z^2(1-z)^2\tilde{q}^2 + m_0^2z(1-z) - m_1^2(1-z) - m_2^2z, \quad (3.3)$$

where on-shell masses, or a cut-off value, $m_{1,2}$ are used for the particles produced in the branching.

As observed in Ref. [26] this choice tends to give too much hard radiation in the parton shower as there is no compensation between the transverse momentum of the branching and the virtualities of the partons produced in the branching.

3.2 q^2 preserving scheme

Ref. [26] suggested that the virtuality of the branching should be determined using the virtualities the particles produced in the branching develop after subsequent evolution, such that

$$p_T^2 = z^2(1-z)^2\tilde{q}^2 + m_0^2z(1-z) - q_1^2(1-z) - q_2^2z. \quad (3.4)$$

Clearly this is the same as Eqn. 3.3 if there is no further emission, *i.e.* $q_{1,2}^2 = m_{1,2}^2$.

This choice, however, has the problem that the subsequent evolution of the partons is not guaranteed to result in a physical, *i.e.* a $p_T^2 \geq 0$, solution of Eqn. 3.4. In Ref. [26] it was noted that the vetoing of emissions that give a non-physical solution affected the logarithmic evolution of the total number of particles. Hence, if there was no physical solution the transverse momentum was set to zero such that the virtuality of the branching particle is

$$q_0^2 = \frac{q_1^2}{z} + \frac{q_2^2}{(1-z)}. \quad (3.5)$$

3.3 Dot-product preserving scheme

Motivated by the original massless angular-ordered parton shower of Ref. [22], where the evolution variable was related to the dot product of the outgoing momenta, we investigate the choice

$$\tilde{q}^2 = \frac{2q_1 \cdot q_2 + m_1^2 + m_2^2 - m_0^2}{z(1-z)}, \quad (3.6)$$

where the inclusion of the masses is required to give the correct propagator in the general case. However, it is not needed for gluon emission, $m_0 = m_1$ and $m_2 = 0$, and only becomes relevant in $g \rightarrow q\bar{q}$ branching.

In this case

$$p_T^2 = z^2(1-z)^2\tilde{q}^2 - q_1^2(1-z)^2 - q_2^2z^2 + z(1-z)[m_0^2 - m_1^2 - m_2^2]. \quad (3.7)$$

As before this reduces to the same result in the case of no further emission.

The major advantage of the original massless algorithm [22] was that the subsequent evolution would always have a physical solution for the transverse momentum. If we consider gluon emission the condition

$$\tilde{q}^2 > 2 \max\left(\frac{q_1^2}{z^2}, \frac{q_2^2}{(1-z)^2}\right), \quad (3.8)$$

is sufficient, but not necessary, for there to be a solution for the transverse momentum in Eqn. 3.7.

If this inequality is satisfied, the virtuality of the branching parton is

$$q_0^2 = q_1^2 + q_2^2 + z(1-z)\tilde{q}^2 \leq \frac{\tilde{q}^2}{2}. \quad (3.9)$$

Assuming that the branching parton was produced in a previous branching, with light-cone momentum fraction z_i and evolution scale \tilde{q}_i , the angular-ordering condition ensures that $\tilde{q} < z_i\tilde{q}_i$. Hence

$$q_0^2 \leq \frac{z_i^2\tilde{q}_i^2}{2}, \quad (3.10)$$

so that if Eqn. 3.8 is satisfied for one branching it will also be satisfied for previous branchings. So provided that we require

$$\tilde{q}^2 > 2 \max\left(\frac{m_1^2}{z^2}, \frac{m_2^2}{(1-z)^2}\right), \quad (3.11)$$

where $m_{1,2}$ are either the physical, or cut-off masses of the partons, the subsequent evolution will be guaranteed to have a physical solution for the transverse momentum.

There are two issues with this choice. The first is that if we impose Eqn. 3.11 on radiation from a heavy quark with mass m , the transverse momentum of the branching must satisfy

$$p_T \geq (1-z)m, \quad (3.12)$$

which, since $p_T \sim (1-z)E\theta$ corresponds to $\theta \geq m/E$, *i.e.* the hard dead-cone [27, 28] the new algorithm was designed to avoid [21]. In practice we use a cut-off on the transverse momentum of the emission which is fine for radiation from gluons and light quarks, and also for the charm quark since the cut-off is close to the charm mass.

For the 3rd generation quarks we get a small fraction of events where the kinematics cannot be reconstructed ($\lesssim 0.2$ per mille and $\lesssim 0.5\%$ of $q \rightarrow qg$ branchings for bottom and top quarks, respectively, hardly varying with centre-of-mass energy). However this region is subleading and therefore we adopt the approach of setting the transverse momentum of the emission to zero as above in this case.

The second, although less important, issue is the $g \rightarrow q\bar{q}$ branching. The limit in this case is presented in Appendix A. For massive quarks, in particular the bottom quark, this limit is stricter than the cut-off on the transverse momentum we use. We therefore have some $g \rightarrow b\bar{b}$ branchings where we are forced to set the transverse momentum to zero. Again this region is subleading ($\lesssim 0.5\%$ of $g \rightarrow b\bar{b}$ branchings, again hardly varying with centre-of-mass energy) and therefore does not affect the logarithmic accuracy.

A full study of these mass effects is beyond the scope of this work, although very important and we hope to return to it in the future.

3.3.1 Phase-space corrections

The angular ordering of the parton shower, which allows a consistent treatment of colour coherence effects, leads to regions of phase space without any gluon emissions. This is the so-called *dead zone*.

The choice of the preserved quantity in presence of multiple emissions can significantly affect the phase-space region which is filled by the shower. Fig. 2 illustrates the Dalitz plot for $e^+e^- \rightarrow q\bar{q}$. We have clustered the partons using the FastJet [29] implementation of the k_T jet algorithm [30] and we have switched off $g \rightarrow q\bar{q}$ splittings in order to unambiguously define the q and \bar{q} jets. We can appreciate how little the q^2 -preserving scheme populates the *dead zone*, coloured in yellow, in opposition to the p_T -preserving scheme. This feature is really crucial when matching to higher order computations, like matrix element corrections, since they will take care to fill this hard region of the phase space. We notice that the dot-product-preserving scheme (bottom-right pane) displays an intermediate behaviour between the two older schemes, with the number of points in the dead zone for the dot-product-preserving scheme about half of that in p_T -preserving scheme.

In order to enforce the similarities between the dot-product preserving scheme and the q^2 one, that is the current **Herwig** default, we implemented a rejection veto to avoid generating too large virtualities. Indeed the virtuality of the shower progenitor, *i.e.* the emitter particle that was present prior to the shower, increases when multiple emissions are generated, while in the q^2 -preserving scheme it is kept fixed. To this end, let us consider the two-body phase space for the process $e^+e^- \rightarrow q\bar{q}$, which reads

$$d\Phi_2(s, m^2, m^2) = \frac{d\Omega}{32\pi^2} \lambda\left(1, \frac{m^2}{s}, \frac{m^2}{s}\right), \quad (3.13)$$

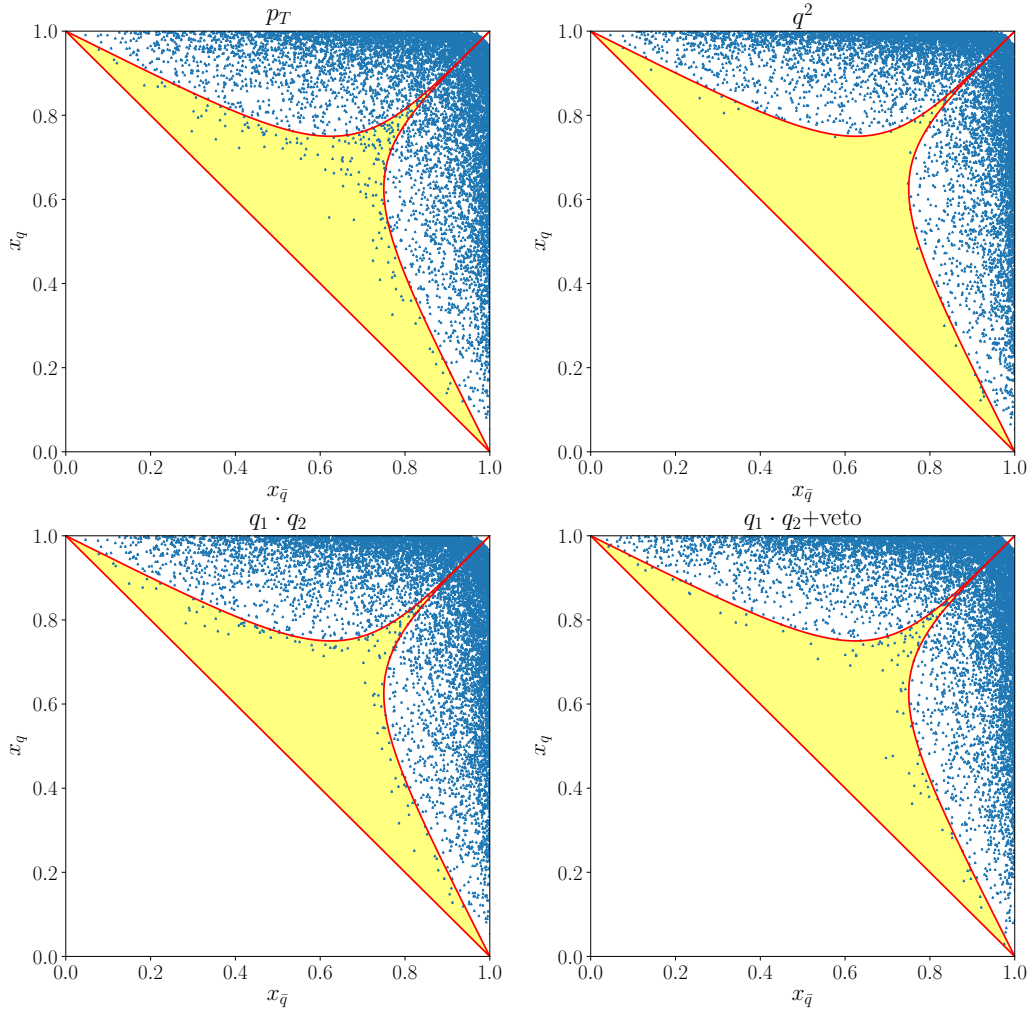


Figure 2. Dalitz plot for $e^+e^- \rightarrow q\bar{q}$ showing the region of phase space filled after multiple emission from the quark and anti-quark in the angular-ordered parton shower for several choices of the preserved quantity: p_T (upper-left pane), q^2 (upper-right pane), dot-product (lower-left pane) and dot-product plus q^2 veto (lower-right pane). The red line illustrates the limits for the first parton-shower emission and the yellow region corresponds to the *dead zone*. The variable x_i is defined to be $2E_i/Q$, where E_i is the energy of parton i and Q is the centre-of-mass energy of the collision.

Ω being the solid angle that describes the direction of the quark. When n emissions are generated the phase space becomes

$$d\Phi_{n+2} = d\Phi_2(s, k_q^2, k_{\bar{q}}^2) \prod_{i=1}^n \frac{d\tilde{q}_i^2}{(4\pi)^2} z_i(1-z_i) dz_i \frac{d\phi_i}{2\pi}, \quad (3.14)$$

where k_l^2 is the virtuality developed by the shower progenitor $l = q, \bar{q}$. Thus, if we want to factorize the phase space over the original two-body one, we need to include

the Jacobian factor

$$J = \frac{d\Phi_2(s, k_q^2, k_{\bar{q}}^2)}{d\Phi_2(s, m^2, m^2)} = \frac{\lambda(s, k_q^2, k_{\bar{q}}^2)}{\lambda(s, m^2, m^2)}. \quad (3.15)$$

Since $J < 1$, we can simply implement a reweighting procedure: at the end of the showering phase we generate a random number r smaller than 1 and we accept the event only if $r < J$, otherwise we shower the event anew. Looking at the Dalitz plots (bottom panel of Fig. 2), we see that while this has only a modest effect, it does somewhat suppress, about a 10% reduction, the events in the dead zone. Note that these plots are all made with the same set of parameters.

4 Logarithmic accuracy

The angular-ordered parton shower has the correct single-emission probability by construction. However it is still instructive to calculate the Lund variables, *i.e.* the transverse momentum k_{\perp} and rapidity y . For a single gluon emission, $m_0 = m_1 = m$ and $m_2 = 0$, all three choices for the interpretation of the evolution variable are identical, giving

$$k_{\perp} = p_T^2 = (1-z)^2 (z^2 \tilde{q}^2 - m^2) \approx z^2 (1-z)^2 \tilde{q}^2 \approx \epsilon^2 \tilde{q}^2, \quad (4.1a)$$

$$y = \frac{1}{2} \ln \left[\frac{(1+b-c+\lambda)^2 Q^2 (1-z)^2}{4p_T^2} \right] \approx \ln \left[\frac{Q(1-z)}{p_T} \right] \approx \ln \left[\frac{Q}{\tilde{q}} \right], \quad (4.1b)$$

where the first approximation is that the radiating particle² is massless, *i.e.* $m \rightarrow 0$, and the second approximation corresponds to soft gluon emission, *i.e.* $z = 1 - \epsilon$ with $\epsilon \rightarrow 0$.

To check the accuracy we need to consider the case of two successive gluon emissions, *i.e.* $m_{0,1,3} = m$, $m_{2,4} = 0$. In particular, in angular-ordered parton showers, one can obtain strongly disordered regions in which a second emission is much harder (in energy, contribution to jet virtuality or transverse momentum) than the first. We therefore have to check that the kinematics of the softer first gluon are not disturbed by the second harder one.

The different schemes only affect the relationship between the transverse momenta and the evolution variable, this means that the kinematics are the same in all three schemes when expressed in terms of the transverse momenta. The Lund

²and the spectator

variables for the two emissions are therefore:

$$k_{\perp 1}^2 = p_{T1}^2; \quad (4.2a)$$

$$y_1 = \frac{1}{2} \ln \left[\frac{(1+b-c+\lambda)^2 Q^2 (1-z_1)^2}{4p_{T1}^2} \right]; \quad (4.2b)$$

$$k_{\perp 2}^2 = (\mathbf{p}_{T2} - (1-z_2)\mathbf{p}_{T1})^2; \quad (4.2c)$$

$$y_2 = \frac{1}{2} \ln \left[\frac{(1+b-c+\lambda)^2 Q^2 z_1^2 (1-z_2)^2}{4k_{\perp 2}^2} \right]. \quad (4.2d)$$

All three choices of evolution variable are identical for one emission, therefore

$$p_{T2}^2 = (1-z_2)^2 [z_2^2 \tilde{q}_2^2 - m^2], \quad (4.3)$$

and the virtuality of the branching parton is

$$q_1^2 = z_2(1-z_2)\tilde{q}_2^2 + m^2. \quad (4.4)$$

For the first branching the relationships depend on our choice of reconstruction scheme.

4.1 p_T preserving scheme

If we use the cut-off scheme

$$p_{T1}^2 = (1-z_1)^2 [z_1^2 \tilde{q}_1^2 - m^2], \quad (4.5)$$

the final virtual mass of the original parton is

$$q_0^2 = \frac{p_{T1}^2}{z_1(1-z_1)} + \frac{q_1^2}{z_1} = z_1(1-z_1)\tilde{q}_1^2 + \frac{z_2(1-z_2)\tilde{q}_2^2}{z_1} + m^2, \quad (4.6)$$

and

$$p_{T2}^2 = (1-z_2)^2 \left(z_2 \sqrt{\tilde{q}_2^2 - \frac{m^2}{z_2^2}} \hat{\mathbf{n}}_2 - z_1(1-z_1) \sqrt{\tilde{q}_1^2 - \frac{m^2}{z_1^2}} \hat{\mathbf{n}}_1 \right)^2, \quad (4.7)$$

where we remind that $\hat{\mathbf{n}}_i$ is a unit vector parallel to \mathbf{p}_{Ti} , see Eqn. (2.10).

In the massless and soft limits, $z_{1,2} \rightarrow 1$ such that $z_{1,2} = 1 - \epsilon_{1,2}$ and $\epsilon_{1,2} \ll 1$, the Lund variables are

$$k_{\perp 1}^2 \approx \epsilon_1^2 \tilde{q}_1^2; \quad (4.8a)$$

$$y_1 \approx \ln \left[\frac{Q}{\tilde{q}_1} \right] \quad (4.8b)$$

$$k_{\perp 2}^2 \approx \epsilon_2^2 (\tilde{q}_2 \hat{\mathbf{n}}_2 - \epsilon_1 \tilde{q}_1 \hat{\mathbf{n}}_1)^2; \quad (4.8c)$$

$$y_2 \approx \frac{1}{2} \ln \left[\frac{Q^2}{(\tilde{q}_2 \hat{\mathbf{n}}_2 - \epsilon_1 \tilde{q}_1 \hat{\mathbf{n}}_1)^2} \right]; \quad (4.8d)$$

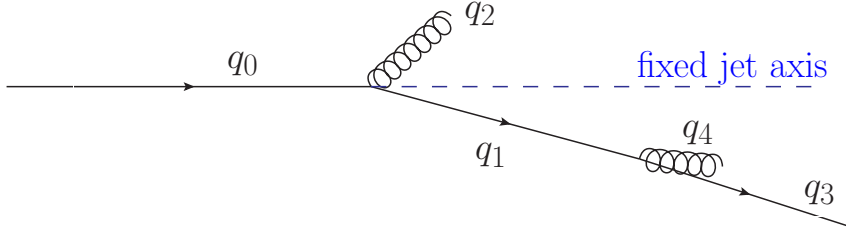


Figure 3. Region in which the emission angle of the second gluon is smaller than the recoil angle of the quark from the first-gluon emission.

In the soft limit

$$q_0^2 = \epsilon_1 \tilde{q}_1^2 + \epsilon_2 \tilde{q}_2^2 + m^2. \quad (4.9)$$

As the limit from angular-ordering is $\tilde{q}_1 \geq \tilde{q}_2$ we see that for

$$\epsilon_2 \tilde{q}_2^2 > \epsilon_1 \tilde{q}_1^2, \quad (4.10)$$

there is a disordered region where the contribution of a second harder gluon to the virtuality of the original parton is dominant. In this disordered region, $k_{\perp 2} \gg k_{\perp 1}$ so that we can neglect $\epsilon_1 \tilde{q}_1$ relative to \tilde{q}_2 and the kinematics are effectively independent. However, there is a region in which the transverse momentum of the first emission overwhelms that of the second, if $\tilde{q}_2 < \epsilon_1 \tilde{q}_1 = k_{\perp 1}$. This is the region in which the emission angle of the second gluon is smaller than the recoil angle of the quark from the first gluon (Fig. 3). It is an issue because we have measured the transverse momentum and rapidity relative to the fixed jet axis, not the local axis of emission³. If we calculate the Lund variables using q_3 as the axis:

$$k_{\perp 1}^2 \approx \epsilon_1^2 (\tilde{q}_1 \hat{\mathbf{n}}_1 + \epsilon_2 \tilde{q}_2 \hat{\mathbf{n}}_2)^2; \quad (4.11a)$$

$$y_1 \approx \frac{1}{2} \ln \left[\frac{Q^2}{(\tilde{q}_1 \hat{\mathbf{n}}_1 + \epsilon_2 \tilde{q}_2 \hat{\mathbf{n}}_2)^2} \right]; \quad (4.11b)$$

$$k_{\perp 2}^2 \approx \epsilon_2^2 \tilde{q}_2^2; \quad (4.11c)$$

$$y_2 \approx \ln \left[\frac{Q}{\tilde{q}_2} \right]. \quad (4.11d)$$

The second gluon variables are as expected. The first gluon variables are correct this time, because \tilde{q}_2 is always smaller than \tilde{q}_1 and the factor of ϵ_2 makes it arbitrarily smaller. Thus, this scheme performs as expected.

³Similar issues were discussed in the context of CAESAR resummation, see Ref. [31] Appendix C.

4.2 q^2 preserving scheme

For the q^2 preserving scheme

$$\begin{aligned} p_{T1}^2 &= \max \left(z_1^2(1-z_1)^2 \tilde{q}_1^2 + m^2 z_1(1-z_1) - q_1^2(1-z_1), 0 \right) \\ &= \max \left((1-z_1) \left[(1-z_1)(z_1^2 \tilde{q}_1^2 - m^2) - z_2(1-z_2) \tilde{q}_2^2 \right], 0 \right), \end{aligned} \quad (4.12)$$

so that the transverse momentum is non-zero if

$$(1-z_1)(z_1^2 \tilde{q}_1^2 - m^2) > z_2(1-z_2) \tilde{q}_2^2. \quad (4.13)$$

In the limit that both $z_{1,2} \rightarrow 1$ then

$$p_{T1}^2 = \max \left(\epsilon_1(\epsilon_1(\tilde{q}_1^2 - m^2) - \epsilon_2 \tilde{q}_2^2), 0 \right), \quad (4.14)$$

so that in the soft limit the transverse momentum is non-zero for massless partons if

$$\epsilon_1 \tilde{q}_1^2 > \epsilon_2 \tilde{q}_2^2, \quad (4.15)$$

which is effectively the requirement that the generated virtualities are ordered, which is clearly violated in the disordered region we are concerned about.

In the ordered region in which a solution is possible, the Lund variables, calculated relative to the q_3 axis are:

$$k_{\perp 1}^2 \approx \epsilon_1^2 \tilde{q}_1^2 - \epsilon_1 \epsilon_2 \tilde{q}_2^2; \quad (4.16a)$$

$$y_1 \approx \frac{1}{2} \ln \left[\frac{Q^2}{\tilde{q}_1^2 - \tilde{q}_2^2 \frac{\epsilon_2}{\epsilon_1}} \right]; \quad (4.16b)$$

$$k_{\perp 2}^2 \approx \epsilon_2^2 \tilde{q}_2^2; \quad (4.16c)$$

$$y_2 \approx \ln \left[\frac{Q}{\tilde{q}_2} \right]. \quad (4.16d)$$

In the bulk of the region, the \tilde{q}_2^2 terms are negligible. However, along the “line” $\epsilon_2 \tilde{q}_2^2 \sim \epsilon_1 \tilde{q}_1^2$ the generated $k_{\perp 1}^2$ value is wrong by a factor of order 1. Moreover, for most reasonable event shapes, *e.g.* thrust, the first gluon is the dominant one. Therefore this is a next-to-leading-logarithmic (NLL) error.

In the disordered region, $p_{T1} = 0$, therefore the Lund variables are:

$$k_{\perp 1}^2 \approx \epsilon_1^2 p_{T2}^2 \approx \epsilon_1^2 \epsilon_2^2 \tilde{q}_2^2; \quad (4.17a)$$

$$y_1 \approx \frac{1}{2} \ln \left[\frac{Q^2}{p_{T2}^2} \right] \approx \frac{1}{2} \ln \left[\frac{Q^2}{\epsilon_2^2 \tilde{q}_2^2} \right]; \quad (4.17b)$$

with $k_{\perp 2}^2$ and y_2 given by Eqn. 4.16. While the kinematics of the second gluon are correct, kinematics of the first gluon are completely wrong in this region in the Lund plane. This could, in principle, be a leading-log effect. However, for the example

of the thrust distribution, in this region the second gluon is the harder gluon and the first gluon makes a sub-leading contribution to the observable. Therefore, again, it is only along the line at the edge of this region that one gets a significant effect and it is a NLL error. We conclude that the q^2 preserving looks undesirable, in reconstructing incorrect kinematics over a finite area of the Lund plane. In practice this leads to a NLL error in the thrust distribution. Related problems with the q^2 preserving scheme were also noted in Ref. [32].

4.3 Dot-product preserving scheme

In the dot-product preserving scheme the mass of the second branching is unchanged but for the first it becomes

$$p_{T1}^2 = z_1^2(1-z_1)^2\tilde{q}_1^2 - q_1^2(1-z_1)^2 = (1-z_1)^2 [z_1^2\tilde{q}_1^2 - z_2(1-z_2)\tilde{q}_2^2 - m^2]. \quad (4.18)$$

The difference relative to Eqn. 4.12 looks minor, but now we have to compare \tilde{q}_1^2 with $\epsilon_2\tilde{q}_2^2$, \tilde{q}_2^2 has to be smaller than \tilde{q}_1^2 and the factor of ϵ_2 makes it parametrically smaller. The second term can therefore never be as large as the first.

The virtuality of the first parton is

$$q_0^2 = \tilde{q}_1^2 z_1(1-z_1) + \tilde{q}_2^2 z_2(1-z_2) + m^2, \quad (4.19)$$

which for soft emissions can be dominated by the second emission for $\epsilon_2 > \epsilon_1$. In this case the transverse momentum of the second branching is

$$p_{T2}^2 = (1-z_2)^2 \left(z_2 \sqrt{\tilde{q}_2^2 - \frac{m^2}{z_2^2}} \hat{\mathbf{n}}_2 - z_1(1-z_1) \sqrt{\tilde{q}_1^2 - \frac{m^2}{z_1^2} - \frac{z_2(1-z_2)\tilde{q}_2^2}{z_1^2}} \hat{\mathbf{n}}_1 \right)^2 \quad (4.20)$$

In the massless and soft limits the Lund variables, with respect to the z axis, are

$$k_{\perp 1}^2 \approx \epsilon_1^2(\tilde{q}_1^2 - \epsilon_2\tilde{q}_2^2); \quad (4.21a)$$

$$y_1 \approx \frac{1}{2} \ln \left[\frac{Q^2}{\tilde{q}_1^2 - \epsilon_2\tilde{q}_2^2} \right] \quad (4.21b)$$

$$k_{\perp 2}^2 \approx \epsilon_2^2(\tilde{q}_2\hat{\mathbf{n}}_2 - \epsilon_1\tilde{q}_1\hat{\mathbf{n}}_1)^2; \quad (4.21c)$$

$$y_2 \approx \frac{1}{2} \ln \left[\frac{Q^2}{(\tilde{q}_2\hat{\mathbf{n}}_2 - \epsilon_1\tilde{q}_1\hat{\mathbf{n}}_1)^2} \right], \quad (4.21d)$$

while with respect to the direction of q_3 they become

$$k_{\perp 1}^2 \approx \epsilon_1^2(\tilde{q}_1^2 + \epsilon_2\tilde{q}_2^2); \quad (4.22a)$$

$$y_1 \approx \frac{1}{2} \ln \left[\frac{Q^2}{\tilde{q}_1^2 + \epsilon_2\tilde{q}_2^2} \right] \quad (4.22b)$$

$$k_{\perp 2}^2 \approx \epsilon_2^2\tilde{q}_2^2; \quad (4.22c)$$

$$y_2 \approx \ln \left[\frac{Q}{\tilde{q}_2} \right]. \quad (4.22d)$$

4.4 Global recoil

We also need to consider the impact of the implementation of the global recoil in Herwig 7. For simplicity we will consider the case of two final-state particles, the generic case can be found in Ref. [25]. We have a particle a with momentum

$$q_a = \sqrt{s} [1, 0, 0, 0], \quad (4.23)$$

which splits into particles b and c , whose momenta are given by

$$p_b = \frac{\sqrt{s}}{2} [1 + b - c, 0, 0, +\lambda(1, b, c)], \quad p_c = \frac{\sqrt{s}}{2} [1 - b + c, 0, 0, -\lambda(1, b, c)], \quad (4.24)$$

where λ is the Källén function defined in eq. (2.4) and $b = m_b^2/s$, $c = m_c^2/s$. During the shower evolution the particles acquire a virtuality $q_b^2 = b's$ and $q_c^2 = c's$ and their momenta are modified

$$q_b = p_b + \beta_b n_b, \quad (4.25)$$

$$q_c = p_c + \beta_c n_c, \quad (4.26)$$

where

$$n_b = \frac{\sqrt{s}}{2} \lambda(1, b, c) [1, 0, 0, -1], \quad n_c = \frac{\sqrt{s}}{2} \lambda(1, b, c) [1, 0, 0, +1], \quad (4.27)$$

and

$$\beta_b = \frac{s(b' - b)}{2p_b \cdot n_b}, \quad \beta_c = \frac{s(c' - c)}{2p_c \cdot n_c}. \quad (4.28)$$

However, if we want to have two particles with invariant mass q_b^2 and q_c^2 , whose three-momentum is parallel to the direction of p_b and p_c respectively, the two particles must have four-momentum equal to

$$q'_b = \frac{\sqrt{s}}{2} [1 + b' - c', 0, 0, +\lambda(1, b', c')], \quad q'_c = \frac{\sqrt{s}}{2} [1 - b' + c', 0, 0, -\lambda(1, b', c')]. \quad (4.29)$$

As $q_b + q_c = q'_b + q'_c$, they can be simply related by a Lorentz transform along the p_b (p_c) direction. The boost parameter for b is

$$\beta^{(b)} = \frac{((b + b')(1 + b - c) + \lambda(b - b'))((b - b')(1 + b - c) + \lambda(b + b')) - 4b^2\lambda'(1 + b' - c')}{((b - b')(1 + b - c) + \lambda(b + b'))^2 + 4b^2(1 + b' - c')^2}, \quad (4.30)$$

where we have used the shorthand notation $\lambda = \lambda(1, b, c)$ and $\lambda' = \lambda(1, b', c')$. The expression may look complicated, but if we consider that b , c , b' and c' are all much smaller than 1, we get

$$\beta^{(b)} \approx c' - c, \quad \beta^{(c)} \approx b' - b. \quad (4.31)$$

Also the partons which have q_b (q_c) as shower progenitor need to be boosted along the direction of the progenitor. This boost will leave the transverse momentum, the light-cone momentum z and the ordering variable \tilde{q} (since it is expressed in terms of scalar products and z) invariant, but not the rapidity of the particles.

Indeed the rapidity of partons having the b as shower progenitor is slightly shift towards smaller values

$$\Delta y_b = \frac{1}{2} \log \left(\frac{1 - \beta^{(b)}}{1 + \beta^{(b)}} \right) \approx -\beta^{(b)}, \quad (4.32)$$

and the rapidity of those coming from the c cascade is slightly pulled in the opposite direction

$$\Delta y_c = \frac{1}{2} \log \left(\frac{1 + \beta^{(c)}}{1 - \beta^{(c)}} \right) \approx \beta^{(c)}, \quad (4.33)$$

where we expand the result because the boost parameter is generally much smaller than 1, being of the order of $(q^2 - m^2)/s$, where q^2 is the virtuality developed by the colour partner of the shower progenitor and m^2 its mass.

Let us now discuss the impact of global recoil for soft emission in the massless limit, *i.e.* for $b = c = 0$. Let us assume for simplicity that b is a quark q and c is an anti-quark \bar{q} . If we use the default **Herwig 7** settings, partons originated from b will all have positive rapidity and the single emission probability in the soft limit is

$$dP_{q \rightarrow qg} = C_F \frac{\alpha_s(p_T)}{2\pi} \frac{d\phi}{2\pi} \frac{dp_T^2}{p_T^2} dy \Theta(y), \quad (4.34)$$

while the probability of a soft-emission originated from c is given by

$$dP_{\bar{q} \rightarrow \bar{q}g} = C_F \frac{\alpha_s(p_T)}{2\pi} \frac{d\phi}{2\pi} \frac{dp_T^2}{p_T^2} dy \Theta(-y), \quad (4.35)$$

and the sum of the two contributions yields

$$dP_{\text{soft}} = C_F \frac{\alpha_s(p_T)}{2\pi} \frac{d\phi}{2\pi} \frac{dp_T^2}{p_T^2} dy. \quad (4.36)$$

However, after we apply our global recoil, the rapidity of the partons gets shifted, to the left for partons coming from b and to the right for those coming from c , causing a double counting of the central-rapidity region. If we call $\bar{\beta}$ the average boost-parameter that is applied after the global recoil, Eq. (4.36) will be modified to

$$dP_{\text{soft}}^{\text{Hw7}} = C_F \frac{\alpha_s(p_T)}{2\pi} \frac{d\phi}{2\pi} \frac{dp_T^2}{p_T^2} dy [1 + \Theta(|y| < \bar{\beta})]. \quad (4.37)$$

Nevertheless, given the fact that $\bar{\beta}$ is of the order q^2/s and for soft emission typically $q^2 \ll s$, this is a power-suppressed effect that does not alter the logarithmic accuracy of the parton shower.

5 Tuning

The new interpretation of the evolution variable means that the hadronization parameters (which are highly sensitive to the PS algorithm) have to be retuned. In order to do so, we follow the same strategy as in Ref. [26]: simulated events are analysed with Rivet [33], which also enables a comparison with experimental results. The dependence on the hadronization and parton shower parameters [34] is interpolated by the Professor program [35], which also finds the set of values which best fit the experimental measurements. Data from LEP1, LEP2, JADE, TASSO and SLD were used, as in the previous study. In our case, where observables were measured by multiple experiments, only the most recent set of data is used. We have not included LHC data in the tuning due to the high CPU-time requirement. We consider only the transverse momentum (p_{Tmin}) and not the virtuality as a cutoff parameter.

Professor offers the possibility to weight each observable differently: we adopted the same weights as in Ref. [26]. Furthermore, as in [26], to prevent the fit being dominated by a few observables with very small experimental uncertainty, we impose a minimum relative error of 5% in the computation of the chi-squared χ^2 .

The following procedure is adopted to tune Herwig 7.

1. First the strong coupling computed in the CMW scheme [24] α_s^{CMW} , the minimum transverse momentum allowed in the showering phase p_T^{min} , and the light quark hadronization parameters are tuned to event shapes, charged-particle multiplicity and identified-particle spectra and rates which only involve light quark hadrons. This class of observables is labelled as “general” in Tab. 2.
2. The hadronization parameters for bottom quarks are then tuned to the bottom quark fragmentation function, event shapes and to the identified-particle spectra from $b\bar{b}$ events.
3. The hadronization parameters involving charm quarks are then tuned to identified-particle spectra and measurements of event shapes from charm events.⁴
4. We then vary one parameter at a time to see if our tune corresponds to the minimum of the χ^2 . In case any where the parameters are significantly displaced from the minimum, we retune them all (this time considering all the experimental distributions for light, bottom and charm quarks together).
5. We repeat the previous step except that now if any parameters are too far from the minimum of the χ^2 , their values are adjusted by hand. In particular, this is needed for bottom quark hadronization parameters like `CIMaxBottom` which Professor is not able to tune: this behaviour was also found in Ref. [26].

⁴Charm parameters are the last to be determined, since charm hadrons are also produced from b -hadron decays.

Preserved	p_T in [26]	q^2 in [26]	p_T	q^2	$q_i \cdot q_j$	$q_i \cdot q_j + \text{veto}$
Light-quark hadronization and shower parameters						
AlphaMZ ($\alpha_s^{\text{CMW}}(M_Z)$)	0.1087	0.1262	0.1074	0.1244	0.1136	0.1186
pTmin	0.933	1.223	0.900	1.136	0.924	0.958
ClMaxLight	3.639	3.003	4.204	3.141	3.653	3.649
ClPowLight	2.575	1.424	3.000	1.353	2.000	2.780
PSplitLight	1.016	0.848	0.914	0.831	0.935	0.899
PwtSquark	0.597	0.666	0.647	0.737	0.650	0.700
PwtDIquark	0.344	0.439	0.236	0.383	0.306	0.298
Bottom hadronization parameters						
ClMaxBottom	4.655	3.911	5.757	2.900	6.000	3.757
ClPowBottom	0.622	0.638	0.672	0.518	0.680	0.547
PSplitBottom	0.499	0.531	0.557	0.365	0.550	0.625
ClSmrBottom	0.082	0.020	0.117	0.070	0.105	0.078
SingleHadronLimitBottom	0.000	0.000	0.000	0.000	0.000	0.000
Charm hadronization parameters						
ClMaxCharm	3.551	3.638	4.204	3.564	3.796	3.950
ClPowCharm	1.923	2.332	3.000	2.089	2.235	2.559
PSplitCharm	1.260	1.234	1.060	0.928	0.990	0.994
ClSmrCharm	0.000	0.000	0.098	0.141	0.139	0.163
SingleHadronLimitCharm	0.000	0.000	0.000	0.011	0.000	0.000

Table 1. The Monte Carlo parameters obtained for different choices of the preserved quantity in the angular-ordered shower.

The values of the default parameters and the new ones we find with our tuning procedure are shown in Tab. 1. The χ^2 per degree of freedom computed with the observables used for the tune, together with some recent data from the ATLAS experiment [36] which is sensitive to both quark and gluon jet properties, are shown in Tab. 2.

From Tab. 1 we can notice that the four reconstruction choices correspond to four significantly different values of the strong coupling, where smaller values correspond to the schemes that give a poorer description of the non-logarithmically enhanced region of the spectrum. The introduction of the veto procedure in the dot preserving scheme indeed induces a 4% enhancement in α_s .

6 Results

In this section we present the results of our simulations, in order to compare the predictions obtained with the several implementations of the recoil discussed above. We first discuss the LEP results, for which *Herwig* provides matrix-element corrections (MEC), and then LHC ones for which *Herwig* does not.

Preserved	p_T	q^2	$q_i \cdot q_j$	$q_i \cdot q_j + \text{veto}$
χ^2 per d.o.f considering several set of observables				
general	4.406	3.152	3.735	3.352
bottom	5.964	6.494	5.127	4.118
charm	2.306	1.725	1.838	1.912
ATLAS jets	0.1598	0.4124	0.1925	0.5396
χ^2 per d.o.f considering sub-samples of the “general” observables				
mult	3.031	2.757	2.822	2.776
event	6.959	3.461	5.191	3.877
ident	10.706	9.950	9.777	10.105
jet	4.579	3.226	4.093	3.638
gluon	1.128	1.174	1.237	1.216
charged	5.439	2.515	3.724	2.856

Table 2. The χ^2 per degree of freedom for different choices of the preserved quantity in the angular-ordered shower, obtained with the distributions we used to tune the light, bottom and charm parameters respectively. The χ^2 corresponding to ATLAS jets, particle multiplicities (mult), event shapes (event), identified-particle spectra (ident), quark jets (jet), gluon jets (gluon) and charged particle distributions (charged) are also shown.

6.1 LEP results

The first event-shape distribution we consider is thrust, Fig. 4. We find the well-known behaviour of the p_T -preserving scheme, which overpopulates the non-logarithmically-enhanced region of phase space that is already filled by MEC and corresponds to the tail of the distribution. Although the dot-product scheme performs better than the p_T one it still overpopulates the *dead zone*, however the description of the tail of the spectrum improves if we include the rejection veto described in Sec. 3.3.1. In the right panel of Fig. 4 an expanded view of the small $1 - T$ region is displayed, where we notice that the new choice of the recoil yields a better agreement with data.

Very similar conclusions can be drawn from the thrust major and minor (Fig. 5) distributions, and from the plots of the C - and D -parameters (Fig. 6). For all the event shape distributions except for D , all the options over-populate the first bin, but the q^2 and dot-product-plus-veto are similar to each other and closest to the data.

Looking at the behaviour of the jet resolution parameter in Fig. 7 we observe that the p_T -scheme most closely matches the data in the large $-\log(y_{23})$ (small y_{23}) tail of the distribution. However, in the small $-\log(y_{23})$ region the q^2 scheme yields a better description of the data. The dot-product scheme with the veto behaves very similar to the q^2 scheme, while the scheme without the veto is similar to the p_T

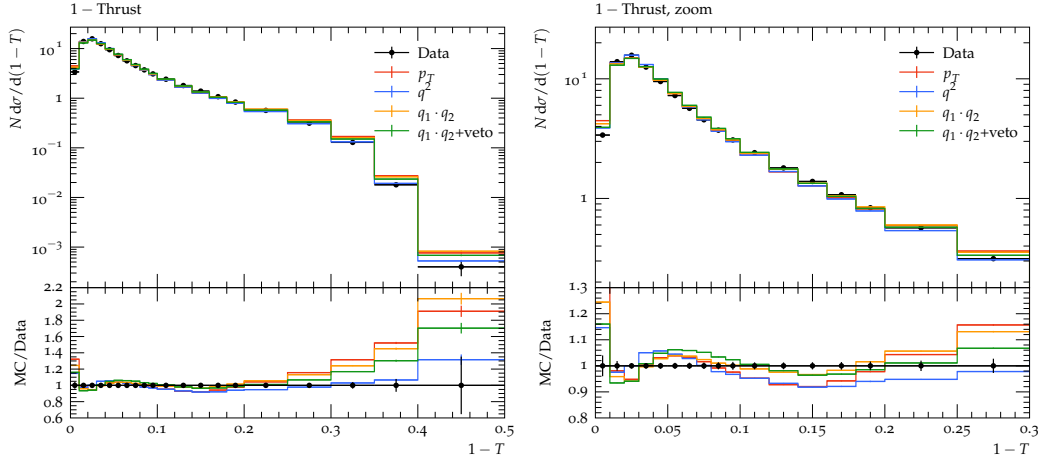


Figure 4. The thrust at the Z-pole compared with data from the DELPHI [37] experiment. In the right panel a zoom for small $1 - T$ values is shown.

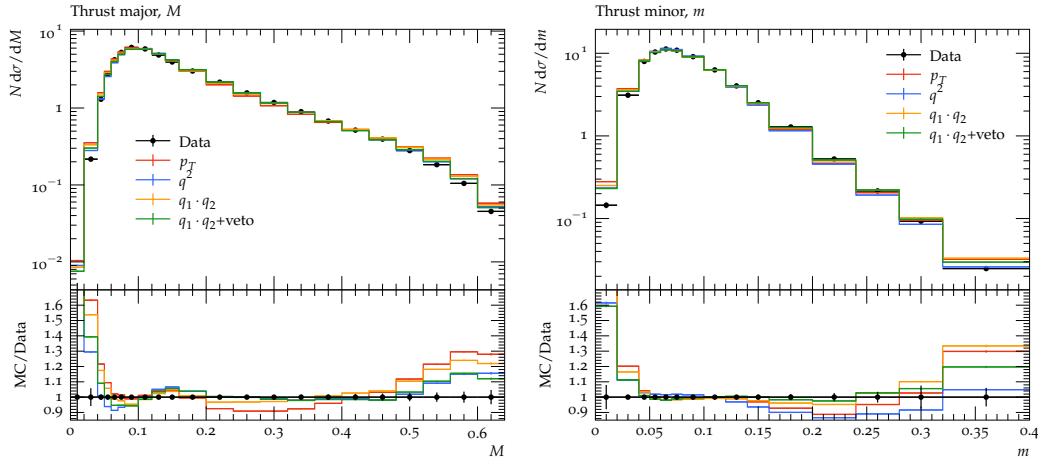


Figure 5. Thrust major (left) and minor (right) at the Z-pole compared with data from the DELPHI [37] experiment.

scheme in the tail of the distribution and to the q^2 one in the opposite limit, thus retaining the best description of the data over the whole range.

In Fig. 8 we show the multiplicity distribution of charged particles in gluons jets for two different gluon energies. We see that the differences between all of the recoil schemes are much smaller than the experimental error and in general they all give a good agreement with the data.

The schemes all fail to describe the peak region of the b fragmentation function, with the different options making little difference, see Fig. 9. Nevertheless, the dot-product-plus-veto scheme gives the best overall description of b data, as can be seen from Tab. 2.

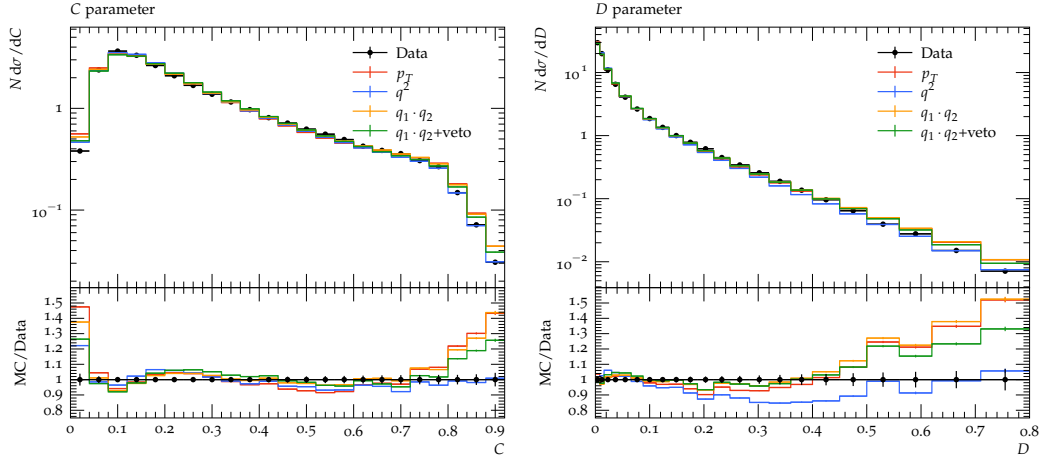


Figure 6. C (left) and D (right) parameters at the Z-pole compared with data from the DELPHI [37] experiment.

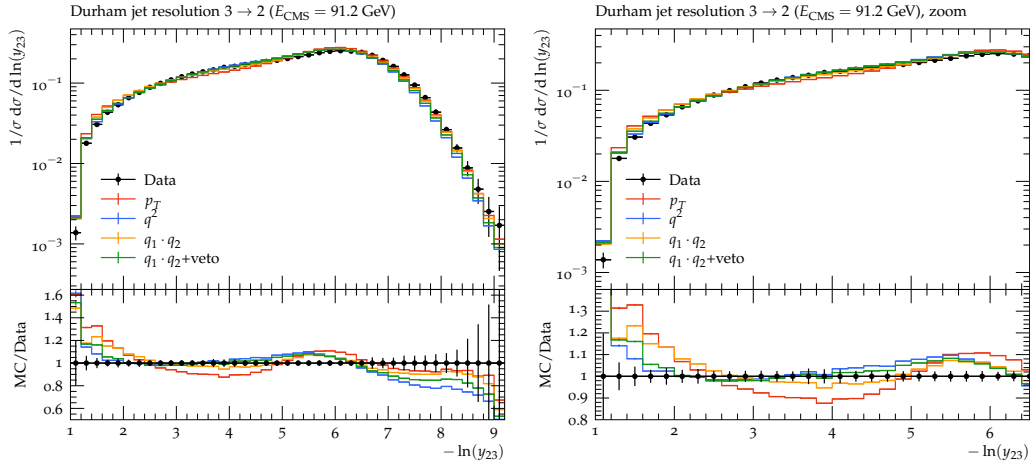


Figure 7. Jet resolution parameter from a 3-jet configuration to a 2-jet configuration at the Z-pole compared with data from the ALEPH [38] experiment. In the right panel an expanded section of the same plot is shown.

6.2 LHC results

Data from jets at the LHC seem to prefer the p_T scheme as shown in Fig. 10. However, this behaviour is due to the absence of MEC in `Herwig` for the events we are simulating. This implies that the dead zone remains unpopulated and the migration of events in this region partially solves the lack of hard emission generation. Nevertheless we do expect that matching with higher order computations will lead to the same behaviour that we find in LEP observables, *i.e.* that the p_T scheme yields too much hard radiation, while for the q^2 scheme, for which the kinematics of subsequent soft emissions are not guaranteed to be independent, we expect worse behaviour in the opposite region of the spectrum, and the dot-product-preserving scheme features intermediate properties.

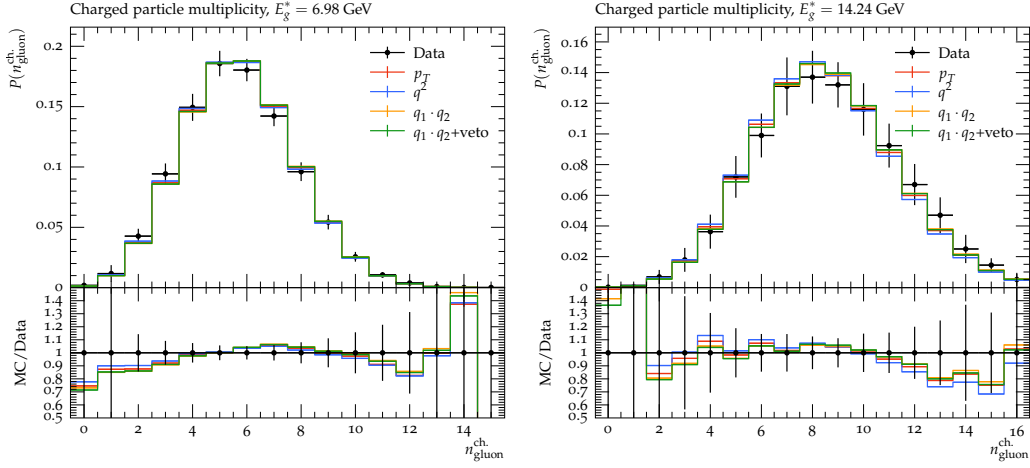


Figure 8. Multiplicity distribution of charged particles in gluon jets for two different gluon energies compared with data from OPAL [39].

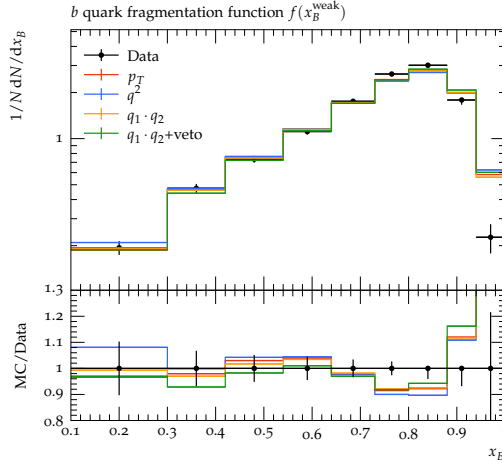


Figure 9. Fragmentation function of weakly-decaying B -hadrons compared with data from DELPHI [40].

7 Conclusions

The pioneering work in Ref. [18] investigated the logarithmic accuracy of dipole showers by focusing on the pattern of multiple emissions. Driven by this work, we have studied how different choices of the recoil scheme in **Herwig** can impact the logarithmic accuracy of the distributions. Furthermore, we also investigated the behaviour of the non-logarithmically-enhanced region of the phase space, that should not be filled by the parton shower, but instead by higher order computations. To this end we proposed an alternative interpretation of the angular-ordering variable that well describes the process of multiple independent soft emission and retain a good agreement with data while also considering the tail of the distributions. In order to enforce the correct behaviour in the hard region of the spectrum, we implemented a

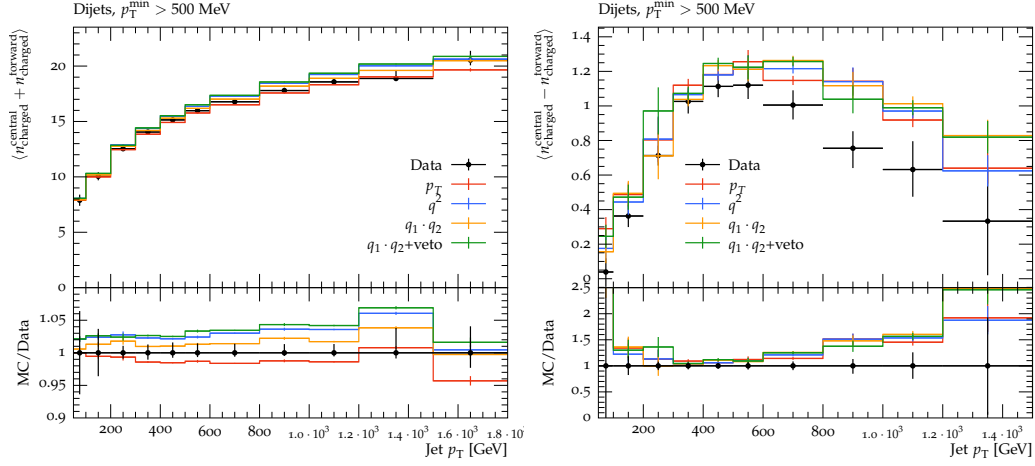


Figure 10. The average number of charged particles in jets (left) and the difference between the average number of particles in central and forward jets (right) as a function of the jet transverse momentum compared with data from the ATLAS experiment [36].

veto that aims to prevent overpopulation of the *dead zone*. This veto applies only to final state radiation and in the future we plan to propose an extension which also includes initial state radiation. In the present work we mainly focused on the case of a massless emitter. The study of mass effects is crucial in assessing the accuracy of the parton shower and will be considered in future works.

Acknowledgments

We thank our fellow Herwig authors for useful discussions, and Johannes Bellm and Bryan Webber for useful comments on the manuscript. This work has received funding from the UK Science and Technology Facilities Council (grant numbers ST/P000800/1, ST/P001246/1), the European Unions Horizon 2020 research and innovation programme as part of the Marie Skłodowska-Curie Innovative Training Network MCnetITN3 (grant agreement no. 722104). GB thanks the UK Science and Technology Facilities Council for the award of a studentship.

A $g \rightarrow q\bar{q}$ branching in the dot-product preserving scheme

In the case of $g \rightarrow q\bar{q}$ branching the transverse momentum of the splitting, Eqn. 3.7, becomes

$$p_T^2 = z^2(1-z)^2\tilde{q}^2 - (q_1^2 - m^2)(1-z)^2 - (q_2^2 - m^2)z^2 - m^2, \quad (\text{A.1})$$

where m is the quark mass. So requiring

$$\tilde{q}^2 > 2 \max \left(\frac{q_1^2 - m^2}{z^2} + \frac{m^2}{2z^2(1-z)^2}, \frac{q_2^2 - m^2}{(1-z)^2} + \frac{m^2}{2z^2(1-z)^2} \right), \quad (\text{A.2})$$

is sufficient, but not necessary, for there to be a physical solution in this case. In this case the virtuality of the branching is

$$q_0^2 = q_1^2 + q_2^2 + z(1-z)\tilde{q}^2 - 2m^2 \leq \frac{\tilde{q}^2}{2}, \quad (\text{A.3a})$$

which again will allow a solution but give a stricter limit.

References

- [1] J. Bellm et al., *Herwig 7.1 Release Note*, [1705.06919](#).
- [2] J. Bellm et al., *Herwig 7.0/Herwig++ 3.0 release note*, *Eur. Phys. J.* **C76** (2016) 196 [[1512.01178](#)].
- [3] T. Sjöstrand, S. Ask, J. R. Christiansen, R. Corke, N. Desai, P. Ilten et al., *An Introduction to PYTHIA 8.2*, *Comput. Phys. Commun.* **191** (2015) 159 [[1410.3012](#)].
- [4] T. Gleisberg, S. Hoeche, F. Krauss, M. Schonherr, S. Schumann, F. Siegert et al., *Event generation with SHERPA 1.1*, *JHEP* **02** (2009) 007 [[0811.4622](#)].
- [5] A. Buckley et al., *General-purpose event generators for LHC physics*, *Phys. Rept.* **504** (2011) 145 [[1101.2599](#)].
- [6] K. Kato and T. Munehisa, *Monte Carlo Approach to QCD Jets in the Next-to-leading Logarithmic Approximation*, *Phys. Rev.* **D36** (1987) 61.
- [7] K. Kato and T. Munehisa, *Double Cascade Scheme for QCD Jets in e^+e^- Annihilation*, *Phys. Rev.* **D39** (1989) 156.
- [8] K. Kato and T. Munehisa, *NLLjet : A Monte Carlo code for e^+e^- QCD jets including next-to-leading order terms*, *Comput. Phys. Commun.* **64** (1991) 67.
- [9] K. Kato, T. Munehisa and H. Tanaka, *Next-to-leading logarithmic parton shower in deep inelastic scattering*, *Z. Phys.* **C54** (1992) 397.
- [10] W. T. Giele, D. A. Kosower and P. Z. Skands, *Higher-Order Corrections to Timelike Jets*, *Phys. Rev.* **D84** (2011) 054003 [[1102.2126](#)].
- [11] L. Hartgring, E. Laenen and P. Skands, *Antenna Showers with One-Loop Matrix Elements*, *JHEP* **10** (2013) 127 [[1303.4974](#)].
- [12] H. T. Li and P. Skands, *A framework for second-order parton showers*, *Phys. Lett.* **B771** (2017) 59 [[1611.00013](#)].
- [13] S. Höche, F. Krauss and S. Prestel, *Implementing NLO DGLAP evolution in Parton Showers*, *JHEP* **10** (2017) 093 [[1705.00982](#)].
- [14] S. Höche and S. Prestel, *Triple collinear emissions in parton showers*, *Phys. Rev.* **D96** (2017) 074017 [[1705.00742](#)].
- [15] F. Dulat, S. Höche and S. Prestel, *Leading-color fully differential two-loop soft corrections to QCD dipole showers*, [1805.03757](#).
- [16] S. Plätzer and M. Sjödal, *Subleading N_c improved Parton Showers*, *JHEP* **07** (2012) 042 [[1201.0260](#)].
- [17] R. A. Martínez, M. De Angelis, J. R. Forshaw, S. Plätzer and M. H. Seymour, *Soft gluon evolution and non-global logarithms*, [1802.08531](#).
- [18] M. Dasgupta, F. A. Dreyer, K. Hamilton, P. F. Monni and G. P. Salam, *Logarithmic accuracy of parton showers: a fixed-order study*, *JHEP* **09** (2018) 033 [[1805.09327](#)].

- [19] T. Sjostrand and P. Z. Skands, *Transverse-momentum-ordered showers and interleaved multiple interactions*, *Eur. Phys. J.* **C39** (2005) 129 [[hep-ph/0408302](#)].
- [20] S. Höche and S. Prestel, *The midpoint between dipole and parton showers*, *Eur. Phys. J.* **C75** (2015) 461 [[1506.05057](#)].
- [21] S. Gieseke, P. Stephens and B. Webber, *New formalism for QCD parton showers*, *JHEP* **12** (2003) 045 [[hep-ph/0310083](#)].
- [22] G. Marchesini and B. R. Webber, *Simulation of QCD Jets Including Soft Gluon Interference*, *Nucl. Phys.* **B238** (1984) 1.
- [23] S. Catani, S. Dittmaier and Z. Trocsanyi, *One loop singular behavior of QCD and SUSY QCD amplitudes with massive partons*, *Phys. Lett.* **B500** (2001) 149 [[hep-ph/0011222](#)].
- [24] S. Catani, B. R. Webber and G. Marchesini, *QCD Coherent Branching and Semi-Inclusive Processes at Large x* , *Nucl. Phys.* **B349** (1991) 635.
- [25] M. Bahr et al., *Herwig++ Physics and Manual*, *Eur. Phys. J.* **C58** (2008) 639 [[0803.0883](#)].
- [26] D. Reichelt, P. Richardson and A. Siodmok, *Improving the Simulation of Quark and Gluon Jets with Herwig 7*, *Eur. Phys. J.* **C77** (2017) 876 [[1708.01491](#)].
- [27] G. Marchesini and B. R. Webber, *Simulation of QCD Coherence in Heavy Quark Production and Decay*, *Nucl. Phys.* **B330** (1990) 261.
- [28] Y. L. Dokshitzer, V. A. Khoze and S. I. Troian, *On specific QCD properties of heavy quark fragmentation ('dead cone')*, *J. Phys.* **G17** (1991) 1602.
- [29] M. Cacciari, G. P. Salam and G. Soyez, *FastJet User Manual*, *Eur. Phys. J.* **C72** (2012) 1896 [[1111.6097](#)].
- [30] S. Catani, Y. L. Dokshitzer, M. Olsson, G. Turnock and B. R. Webber, *New clustering algorithm for multi - jet cross-sections in $e^+ e^-$ annihilation*, *Phys. Lett.* **B269** (1991) 432.
- [31] A. Banfi, G. P. Salam and G. Zanderighi, *Principles of general final-state resummation and automated implementation*, *JHEP* **03** (2005) 073 [[hep-ph/0407286](#)].
- [32] A. H. Hoang, S. Plätzer and D. Samitz, *On the Cutoff Dependence of the Quark Mass Parameter in Angular Ordered Parton Showers*, *JHEP* **10** (2018) 200 [[1807.06617](#)].
- [33] A. Buckley, J. Butterworth, L. Lonnblad, D. Grellscheid, H. Hoeth, J. Monk et al., *Rivet user manual*, *Comput. Phys. Commun.* **184** (2013) 2803 [[1003.0694](#)].
- [34] J. Bellm, D. Grellscheid, P. Kirchgaerber, A. Papaefstathiou, S. Plätzer, M. Rauch et al., "The physics of herwig 7."
- [35] A. Buckley, H. Hoeth, H. Lacker, H. Schulz and J. E. von Seggern, *Systematic event generator tuning for the LHC*, *Eur. Phys. J.* **C65** (2010) 331 [[0907.2973](#)].

- [36] ATLAS collaboration, G. Aad et al., *Measurement of the charged-particle multiplicity inside jets from $\sqrt{s} = 8$ TeV pp collisions with the ATLAS detector*, *Eur. Phys. J.* **C76** (2016) 322 [[1602.00988](#)].
- [37] DELPHI collaboration, P. Abreu et al., *Tuning and test of fragmentation models based on identified particles and precision event shape data*, *Z. Phys.* **C73** (1996) 11.
- [38] ALEPH collaboration, A. Heister et al., *Studies of QCD at e^+e^- centre-of-mass energies between 91-GeV and 209-GeV*, *Eur. Phys. J.* **C35** (2004) 457.
- [39] OPAL collaboration, G. Abbiendi et al., *Experimental studies of unbiased gluon jets from e^+e^- annihilations using the jet boost algorithm*, *Phys. Rev.* **D69** (2004) 032002 [[hep-ex/0310048](#)].
- [40] DELPHI collaboration, J. Abdallah et al., *A study of the b-quark fragmentation function with the DELPHI detector at LEP I and an averaged distribution obtained at the Z Pole*, *Eur. Phys. J.* **C71** (2011) 1557 [[1102.4748](#)].